Supporting Information

Gajiwala *et al.* 10.1073/pnas.0812413106

SI Methods

Cloning and Protein Purification. Briefly, for structural biology and biochemical studies, a construct encoding an N-terminal 6×-His tag + r3c protease site + KIT residues 544–693 + Thr-Ser + KIT residues 694–944 was cloned into baculovirus expression vector pVL1393. The construct used in biochemical assays encoded an N-terminal 6×-His tag + r3c protease site + KIT residues 544–976. High-titer viral stocks were made and proteins were expressed in Sf9 cells at a multiplicity of infection of one for 48 h. Cells were harvested and frozen at −80 °C. The pellet was lysed in 25 mM Tris (pH 7.4), 250 mM NaCl, 0.25 mM TCEP, and 20 mM imidazole and bound to a Ni-NTA column. The protein was step-eluted using the same buffer with 250 mM imidazole. Peak fractions were dialyzed overnight at 4 °C and the His tag cleaved with r3C protease. Protein was reloaded on Ni-NTA to remove the cleaved His tag. Flow-through was collected from the column and concentrated. Protein was run on a Superdex-200 column equilibrated in 25 mM Tris (pH 7.4), 250 mM NaCl, 0.5 mM TCEP, and 1 mM EDTA. Peak fractions were pooled, concentrated to 6 mg/mL, and flash-frozen.

Kinase Activity Assay. Activated KIT was prepared by incubating 10 μM unactivated KIT with 4 mM ATP in Buffer A [50 mM Hepes (pH 7.5), 10 mM $MgCl_2$, 1 mM EGTA, 3 μM Na_3VO_4, 0.1% Brij-35] for 3 h at room temperature. The activated enzyme was then stored at −80 °C for future use. KIT kinase activity was determined using a coupled assay method in an ATP-regenerating system as described previously (17) with slight modification. The assay was typically run for 1 h in a 100-μL assay mixture containing 1.2 mM ATP, 3 mM phosphoenolpyruvate, 0.5 mM NADH, 0.25 mg/mL poly(Glu-Tyr), 25 units pyruvate kinase, and 31 units lactate dehydrogenase in Buffer A. The steady-state rate of poly(Glu-Tyr) phosphorylation was computed from the observed linear decrease in absorbance at 340 nm (A_{340}) due to the coupled oxidation of NADH, using 6220 nm as the molar absorbance of NADH. In the absence of phosphor-acceptor poly(Glu-Tyr), NADH depletion was negligible.

Crystallization and Structure Determination. X-ray data were collected at −175 °C at Advanced Light Source beamlines 5.0.1 and 5.0.2. Structures were determined by molecular replacement using the published structure of autoinhibited KIT (PDB ID code 1T45) as the starting model.

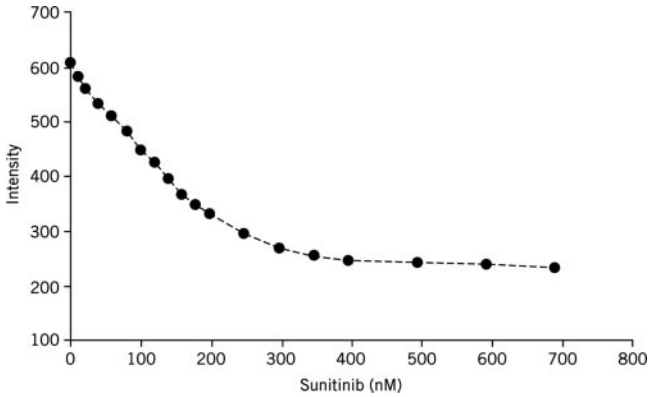

Fig. S1. Quenching of unactivated WT KIT protein fluorescence by sunitinib. ≈200 nM WT KIT protein with JM domain was titrated with increasing concentrations of sunitinib using the same buffer as used for the enzyme activity assay. The protein fluorescence observed at 340 nm after each addition of drug was plotted against the concentration of sunitinib, and the data were fitted to the Morrison equation for tight-binding inhibitors to obtain the K_ds shown in Table 1.

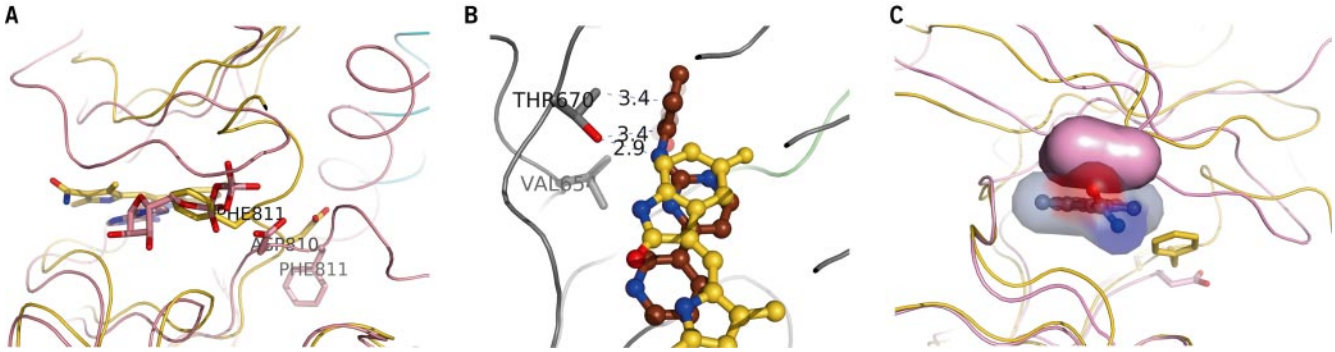

Fig. S2. Sunitinib binding to WT KIT. (*A*) The ATP-binding pocket of the sunitinib-bound KIT structure (yellow) is shown superposed on the ADP-bound activated KIT structure (pink) (7). Asp-810 and Phe-811 of the DFG triad are shown for both structures. The activated structure exemplifies the canonical DFG-in conformation, whereas the sunitinib-bound structure shows the catalytically incompetent DFG state in which Phe-811 protrudes into the ATP-binding pocket. (*B*) Superposition of sunitinib binding on the published imatinib-bound KIT structure (8). Whereas imatinib (brown) makes intimate contacts with Thr-670, sunitinib (yellow) does not access the immediate neighborhood of Thr-670, which explains why mutation of Thr-670 to Ile at the back of the ATP-binding pocket renders the kinase resistant to imatinib but not to sunitinib. (*C*) Steric conflict between sunitinib and the glycine-rich loop of activated KIT. Sunitinib-bound autoinhibited KIT (yellow) is superposed on the structure of the activated enzyme (pink) (7). Steric conflict between the surface representations of Leu-595 side chain and the drug could be one of the reasons for the poor drug sensitivity of the activated state.

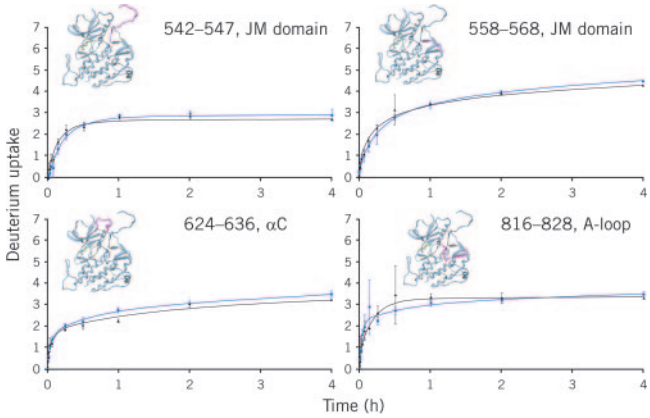

Fig. S3. Time courses of HDX for WT KIT with bound sunitinib with (blue) or without the KID (black) showed no significant conformational differences in the JM domain (residues 542–586), the αC segment (residues 624–636), or the A-loop (residues 810–834).

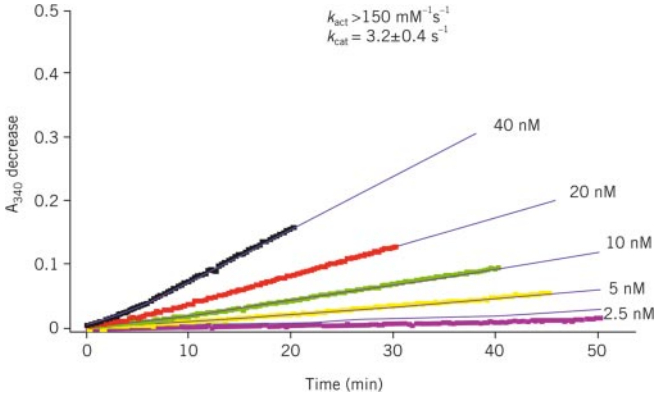

Fig. S4. JM-domain mutant V560D and mutant V560D + T6701 autoactivates at the highest rate of all mutants studied. Autoactivation was monitored and k_{act} derived as described in the legend to Fig. 5.

Table S1. Crystallization data collection and refinement statistics

	WT KIT	D816H KIT
Data collection		
Space group	$P2_12_12_1$	$P2_12_12$
Cell dimensions		
a, *b*, *c*; Å	48.03, 80.97, 93.32	79.46, 101.78, 105.50
α, β, γ; °	90, 90, 90	90, 90, 90
Resolution, Å	20–1.6 (1.66–1.6)*	20–2.6 (2.69–2.6)*
R_{sym} or R_{merge}	0.039 (0.241)	0.042 (0.216)
$I/\sigma I$	31.8 (6.6)	30.0 (7.6)
Completeness, %	99.7 (100)	99.2 (96.8)
Redundancy	4.9 (5.0)	4.6 (4.2)
Refinement		
Resolution; Å	2–1.6	2–2.6
No. of reflections	48,536	26,729
R_{work}/R_{free}	0.200/0.212	0.205/0.256
No. of atoms	3,023	4,724
Protein	2,685	4,660
Ligand/ion	22	49
Water	316	15
B-factors		
Protein	18.7	51.6
Ligand/ion	16.6	37.8
Water	26.2	40.8
R.m.s. deviations		
Bond lengths, Å	0.004	0.006
Bond angles, °	0.788	0.908

Single crystals were used for each structure.
*Values in parentheses are for highest-resolution shell.